Monitoring the Spatial Distribution of High-Resolution Leaf Area Index Using Observations From DMC+4

Jin Huiran, Tao Xin, Fan Wenjie, Xu Xiru, Li Peijun
Institute of Remote Sensing and Geographic Information System
Peking University
Beijing, China
hrjin@pku.edu.cn

***Abstract*—Monitoring the sowing area and the crops growth are the two basic aspects of agricultural remote sensing. With the advantage of DMC+4 simultaneously providing mid-resolution multispectral image and high-resolution panchromatic image, we choose winter wheat as investigated object, establish a vegetation canopy radiation model on the consider of sun-target-sensor geometry and clumping effect to monitor the spatial distribution of the growth condition of winter wheat, and then validate the model through mathematical simulation and field experiment. The work indicates that the model and retrieval method used are available. The spatial scaling effect of LAI is to be further studied.**

Keywords-DMC+4; vegetation canopy radiation model; LAI spatial distribution

I. INTRODUCTION

Monitoring the sowing area and the crops growth are the two basic aspects of agricultural remote sensing. Leaf Area Index (LAI) is the most fundamental parameter for indicating the growth condition of vegetation canopy. Nowadays, in order to retrieve LAI, the retrieval methods mainly bases on multispectral data, according to the unique spectral character of vegetation, and uses experiential or physical models [1-7]. However, since cropland is relatively cracked in China, if mid-resolution or low-resolution images are used to estimate LAI, the error might be large as large numbers of mixed pixels exist. With high-resolution panchromatic data, although we may avoid the influence of mixed pixel on a large degree, even evaluate the sowing area directly from eyes judgment, we can't get any accurate information about LAI. Therefore, we try to combine the respective advantage of mid-resolution multispectral data and high-resolution panchromatic data, so as to gain the spatial distribution information of LAI in high-resolution image, which is the main issue of this study.

With the start using of Disaster Monitoring Constellation +4 (DMC+4), it's more possible to solve the problem. DMC+4 is an earth observing micro-satellite with two sensors. It was set up successfully in Plesetst, Russia on October 27, 2005. This micro-satellite has a unique advantage of simultaneously providing 32 meter mid-resolution multispectral information, containing green (520nm-620nm), red (630nm-690nm) and near infrared (760nm-900nm) three bands, and 4 meter high-resolution panchromatic information, from 500nm to 800nm, thus the geometric relation among sun-target-sensor is the same [8-9]. Multispectral data is helpful to get average LAI in a pixel, while panchromatic data can be used to monitor sowing area of crops accurately. In this study, we choose winter wheat as investigated object, establish a vegetation canopy radiation model on consider of sun-target-sensor geometry and clumping effect to retrieve the LAI spatial distribution of high-resolution panchromatic image properly. The following mathematical simulation and field experiment indicate that the model and retrieval method used are available.

II. THEORY

A. Vegetation Canopy Radiation Model

We choose winter wheat as investigated object. Radiance can be described by the sum of single and multiple scattering,

$$L = L^1 + L^m . \quad (1)$$

The cropland is continuous along row, but discrete in the vertical direction, so it has two combined characteristics. Observation shows that illuminated ground and canopy, as well as shadow ground and canopy can all be seen from sensors. In other words, the bidirectional reflectance effect caused by the geometry of sun-target-sensor is still a primary factor that should be considered.

Radiance of single scattering received is,

$$L^1 = K_g L_g + K_c L_c + K_z L_z + K_t L_t \quad (2)$$

$$K_g + K_c + K_z + K_t = 1 \quad (3)$$

where L_g, L_c, L_z, L_t represent radiance of illuminated ground and canopy, as well as shadow ground and canopy respectively, and K_g, K_c, K_z, K_t represent the area ratios of the four parts same with Geometric-Optical model [10-12]. Each L can be written as

$$L_g = f_g(\mu_s F_0 + E_d), \quad L_z = f_g E_d$$
$$L_c = f_c(\mu_s F_0 + E_d), \quad L_t = f_c E_d \quad (4)$$

where f_g, f_c stand for BRDF of ground and canopy. F_0 is the direct irradiance of sun, and E_d is the diffuse irradiance of

National High-Tech Development Program (863), No.2005AA133011XZ07.
National Natural Science Foundation of China, No. 40401036

atmosphere. $\mu_s = \cos\theta_s$, θ_s is the solar zenith angle. The sum of K_g and K_z expresses the gap probability of canopy,

$$K_g + K_z = e^{-\frac{G(\Omega_v)}{\mu_v} \cdot LAI} \tag{5}$$

According to the principle of Boolean [13-14],

$$K_g = e^{-LAI\left[\frac{G(\Omega_s)}{\mu_s} + \frac{G(\Omega_v)}{\mu_v} - \bar{K}(\theta_s,\theta_v)\right]} \tag{6}$$

Here $\mu_v = \cos\theta_v$, θ_v is the viewing zenith angle. G Function describes the abridged proportion through collision, and $\bar{K}(\theta_s,\theta_v)$ is the probability of overlapping projection in solar and viewing directions.

Now we use a simple linear function $\Gamma(\phi)$ to simplify (6), here ϕ is the angle between light and viewing projection directions. $\Gamma(\phi)$ takes values as follows: when $\phi = 0$, $\Gamma(0) = 1$, when $\phi = \pi$, $\Gamma(\pi) = 2$, when $0 < \phi \le \pi$,

$$\Gamma(\phi) = 1 + \frac{\phi}{\pi} \tag{7}$$

$$K_g = e^{-\frac{G(\Omega_v)}{\mu_v} \cdot LAI \cdot \Gamma(\phi)} \tag{8}$$

In fact, $\Gamma(\phi)$ is used to correct the effect of shadow. When $\phi = 0$, the sensor is at the hot spot location, and $\frac{G(\Omega_v)}{\mu_v} = \frac{G(\Omega_s)}{\mu_s} = \bar{K}(\theta_s,\theta_v)$, so $\Gamma(0) = 1$ is correct. When $\phi = \pi$, projections from two different directions are no longer overlapped, and $\bar{K}(\theta_s,\theta_v) = 0$. Suppose $\frac{G(\Omega_v)}{\mu_v} \cong \frac{G(\Omega_s)}{\mu_s}$, and $\Gamma(\pi) = 2$. For row-crops, even if the geometry of sun-target-sensor is known, we cannot confirm ϕ values, as the average ridge direction of each pixel is indefinite, so

$$K_z = e^{-\frac{G(\Omega_v)}{\mu_v} \cdot LAI} - e^{-\frac{G(\Omega_v)}{\mu_v} \cdot LAI \cdot \Gamma(\phi)} \tag{9}$$

At the hot spot location, any leaves in shadow will not be observed. As ϕ increases, the area of illuminated canopy decreases step by step. Equation (10) and (11) is used to represent this variation approximately.

$$K_c = 1 - e^{-\frac{G(\Omega_v)}{\mu_v} \cdot LAI \Big/ \Gamma(\phi)} \tag{10}$$

$$K_t = 1 - K_g - K_z - K_c = e^{-\frac{G(\Omega_v)}{\mu_v} \cdot LAI \Big/ \Gamma(\phi)} - e^{-\frac{G(\Omega_v)}{\mu_v} \cdot LAI}. \tag{11}$$

Many scientists have pointed out that LAI values retrieved are different by sensors with different resolution. Analysis shows that heterogeneity and non-linear algorithms are the basic reasons for spatial scaling problem. In canopy scale, the clumping effect is another important factor that cannot be neglected in order to achieve accurate LAI retrieval. Therefore, Nilson parameter (λ_0) is used to describe foliage's clumping effect. If foliage is clumpy distributed, $\lambda_0 < 1$, and true value of LAI equals the product of λ_0 and the retrieved value [15].

λ_0 may be different for each pixel. Thus, equations above should be changed as follows,

$$K_g = e^{-\lambda_0 \cdot \frac{G(\Omega_v)}{\mu_v} \cdot LAI \cdot \Gamma(\phi)} \tag{12}$$

$$K_c = 1 - e^{-\lambda_0 \cdot \frac{G(\Omega_v)}{\mu_v} \cdot LAI \Big/ \Gamma(\phi)} \tag{13}$$

$$K_z = e^{-\lambda_0 \cdot \frac{G(\Omega_v)}{\mu_v} \cdot LAI} - e^{-\lambda_0 \cdot \frac{G(\Omega_v)}{\mu_v} \cdot LAI \cdot \Gamma(\phi)} \tag{14}$$

$$K_t = e^{-\lambda_0 \cdot \frac{G(\Omega_v)}{\mu_v} \cdot LAI \Big/ \Gamma(\phi)} - e^{-\lambda_0 \cdot \frac{G(\Omega_v)}{\mu_v} \cdot LAI}. \tag{15}$$

Since heterogeneity is weakened by multiple scattering, L^m can be represented with the two stream approximation of any radiative transfer theory [16-18], which is a function of LAI.

Suppose $\rho^1 = \frac{\pi L^1}{\mu_0 F_0 + E_d}$, $\rho^m = \frac{\pi L^m}{\mu_0 F_0 + E_d}$, $\rho_g = \pi f_g$, $\rho_c = \pi f_c$, so $\rho = \rho^1 + \rho^m$,

$$\rho = \rho^m + \rho_g \left\{ e^{-\lambda_0 \cdot \frac{G(\Omega_v)}{\mu_v} \cdot LAI \cdot \Gamma(\phi)} + \left[e^{-\lambda_0 \cdot \frac{G(\Omega_v)}{\mu_v} \cdot LAI} - e^{-\lambda_0 \cdot \frac{G(\Omega_v)}{\mu_v} \cdot LAI \cdot \Gamma(\phi)} \right] \frac{E_d}{\mu_0 F_0 + E_d} \right\} +$$
$$\rho_c \left\{ \left(1 - e^{-\lambda_0 \cdot \frac{G(\Omega_v)}{\mu_v} \cdot LAI \Big/ \Gamma(\phi)} \right) + \left[e^{-\lambda_0 \cdot \frac{G(\Omega_v)}{\mu_v} \cdot LAI \Big/ \Gamma(\phi)} - e^{-\lambda_0 \cdot \frac{G(\Omega_v)}{\mu_v} \cdot LAI} \right] \frac{E_d}{\mu_0 F_0 + E_d} \right\} \rho^m \tag{16}$$

Here, ρ_g, ρ_c can be replaced by values from field measurement or spectral library. Suppose $G(\Omega_v) \equiv \frac{1}{2}$, which means leaves are randomly oriented, and $E_{d,0.5\mu m} = 0.1 \cdot F_{0,0.5\mu m}$, for other wave bands,

$$\frac{E_{d,\lambda}}{E_{d,0.5\mu m}} = \left(\frac{0.5}{\lambda} \right)^{-4} \tag{17}$$

Equation (16) is the basic formula for LAI retrieval. It reserves almost all the influential factors, such as spectrum characteristics of ground and canopy, LAI, clumping effect of different scales, BRDF and so on. Therefore, it's neither a pure geometric-optical model, nor a traditional radiation transfer model, but a cross model suitable for row-crop, which owns both the continuous and discrete characters. It can be used for different wavelengths, and easy for inversion.

B. Mathematical Simulation

The image of Enhanced Thematic Mapper Plus (ETM+) has six 30m multispectral bands and a 15m panchromatic one. Owing to its abundant information, stable parameters and plentiful applications, as well as integrated field data derived synchronously with the satellite, we choose an ETM+ image of Shunyi District, Beijing on May 19, 2001, to justify the model through a mathematical simulation. After completing radiation calibration work, Brightness (B) and Greenness (G) of each pixel are acquired by the experiential K-T Transform formula, a compact expression of vegetation. The result is shown on a B-G figure.

In addition, equation (16) only contains three unknowns, which are LAI, ϕ and λ_0. Average λ_0 is settled through a

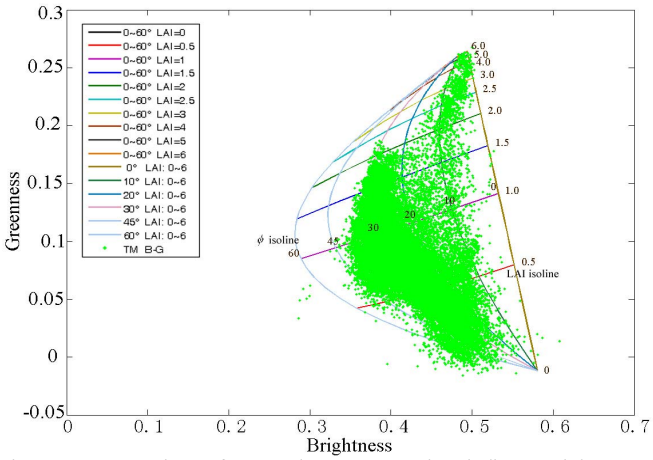

Figure 1. Comparison of B-G values. Green points indicate Brightness and Greenness calculated by the experiential K-T Transform formula for TM image. Colorful lines indicate ϕ isolines and LAI isolines based on (16).

few groups of field and remote sensed data. Let LAI be a certain value, for each different ϕ, we successfully calculate six multispectral reflectance using (16), and then get B and G of each pixel. Change LAI to a few different values and repeat the process. Thus it is feasible to draw some LAI isolines. Similarly, make ϕ constant and alter LAI each time, we gain several ϕ isolines. Fig.1 shows comparison between the results from experiential formula and the model we set up.

As long as B and G are known, LAI can be interpolated from Fig.1. The values agree with field measurements on the whole. Therefore, we can conclude that the vegetation canopy radiation model set up above is basically competent and effective.

III. RESULTS

A. *Retrieval of Winter Wheat LAI Spatial Distribution From DMC+4 Data*

Select a 32m multispectral image and a 4m panchromatic image. The sizes of the two images are both 3.2km×3.2km, simultaneously acquired from DMC+4 in Taian, Shandong Province on March 31, 2006. Some preprocessing work is necessary. Make the two images matching precisely and perform radiation calibration to each band at first [19]. After atmosphere corrections using 6S code to get actual surface reflectance, the high-resolution panchromatic image also needs cross radiation correction, which is helpful to compensate high frequency information and enhance the image definition.

For the three multispectral bands, there are four independent equations as follows,

$$\begin{cases} \rho_{\text{green}} = \rho_{\text{g,green}}\left(K_{\text{g}} + K_{\text{z}}\dfrac{E_{\text{d},\lambda}}{\mu_0 F_0 + E_{\text{d},\lambda}}\right) + \rho_{\text{c,green}}\left(K_{\text{c}} + K_{\text{t}}\dfrac{E_{\text{d},\lambda}}{\mu_0 F_0 + E_{\text{d},\lambda}}\right) \\ \rho_{\text{red}} = \rho_{\text{g,red}}\left(K_{\text{g}} + K_{\text{z}}\dfrac{E_{\text{d},\lambda}}{\mu_0 F_0 + E_{\text{d},\lambda}}\right) + \rho_{\text{c,red}}\left(K_{\text{c}} + K_{\text{t}}\dfrac{E_{\text{d},\lambda}}{\mu_0 F_0 + E_{\text{d},\lambda}}\right) \\ \rho_{\text{ir}} = \rho_{\text{g,ir}}\left(K_{\text{g}} + K_{\text{z}}\dfrac{E_{\text{d},\lambda}}{\mu_0 F_0 + E_{\text{d},\lambda}}\right) + \rho_{\text{c,ir}}\left(K_{\text{c}} + K_{\text{t}}\dfrac{E_{\text{d},\lambda}}{\mu_0 F_0 + E_{\text{d},\lambda}}\right) \\ K_{\text{g}} + K_{\text{z}} + K_{\text{c}} + K_{\text{t}} = 1 \end{cases} \quad (18)$$

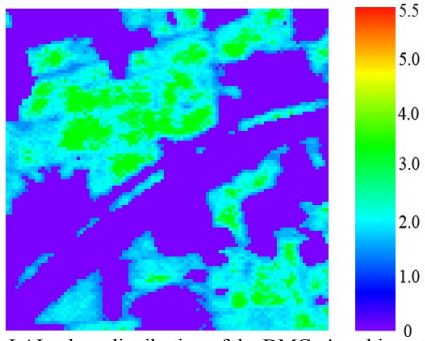

Figure 2. LAI values distribution of the DMC+4 multispectral image

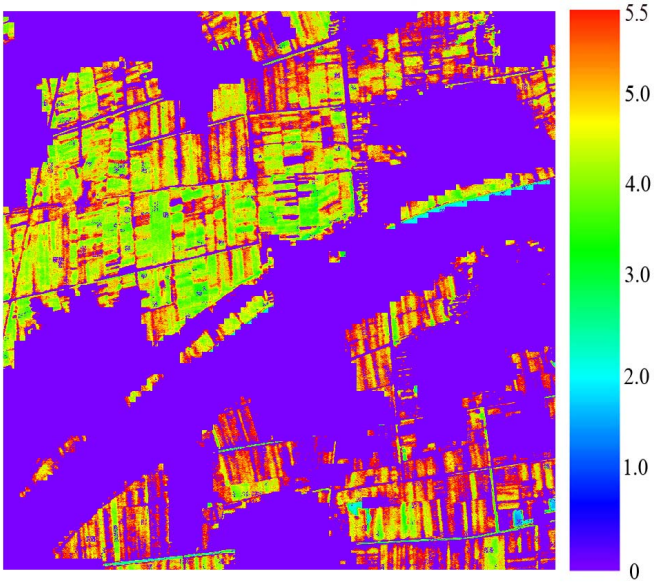

Figure 3. LAI values distribution of the DMC+4 panchromatic image

where each F_0 is the value settled from radiation calibration, and $\rho_{\text{g},\lambda}, \rho_{\text{c},\lambda}$ are read out from spectral library. Ignore multi-scattering and solve the linear equations to get values of $K_{\text{g}}, K_{\text{z}}, K_{\text{c}}, K_{\text{t}}$. Then LAI, ϕ and λ_0 of each multispectral pixel can be calculated out. Fig.2 shows LAI values distribution of the DMC+4 multispectral image.

Since values of ϕ and λ_0 are similar in corresponding sites, we use every ϕ and λ_0 derived above to describe relevant panchromatic pixels. Try to get $\rho_{\text{g}}, \rho_{\text{c}}$, reflectance of pure ground and canopy pixel, from image. Consequently, according to (16), we finally succeed in calculating LAI values of 4m resolution pixels. Fig.3 shows LAI values distribution of the DMC+4 panchromatic image.

B. *Accurancy Analysis*

We evaluate these retrieval results through a Landsat-5 image acquired in Shandong Province on April 29, 2005, as field measurement data is short in the district DMC+4 covers, but sufficient to TM image. Fig.4 shows the comparison of LAI retrieved by (16) from DMC+4 and TM images. The relation is approximately linear. In Fig.4, we also find out that LAI values are all concentrated from 3 to 6. Since the Landsat-5 image is received a few days latter, it is reasonable that its LAI values are generally higher than the other.

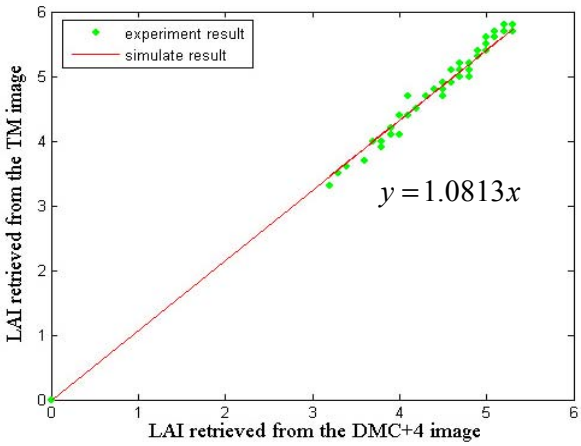

Figure 4. Comparison of retrieved LAI from DMC+4 and TM images

Table 1 is the contrast of LAI values between field measurements and retrievals from TM image. The errors keep within 10%. Both Fig.4 and Table I demonstrate the vegetation canopy radiation model we set up is applied to DMC+4 data, and can be used to retrieve LAI of mixed pixels more accurately as well.

TABLE I. CONTRAST OF LAI VALUES

	LAI values				
Field measure	4.49 ±0.14	4.95 ±0.17	5.11 ±0.17	6.19 ±0.23	6.05 ±0.06
Retrieve	4.50	4.98	5.10	5.83	5.67

IV. CONCLUSIONS

In this study, we establish a vegetation canopy radiation model to express both the continuous and discrete characteristics of winter wheat, which can use the advantage of DMC+4 simultaneously providing 32m mid-resolution multispectral information and 4m high-resolution panchromatic information. This model reserves basic spectrum characteristics of vegetation, and is simple for application. Comparison with a TM image and some field measurements indicates that the error keeps within 10%, thus the accuracy is satisfied. Therefore, it is a new useful LAI retrieving method suitable for row-crops.

It is a distinctive character of DMC+4 that providing multispectral and panchromatic data simultaneously, and the geometric relation among sun-target-sensor is the same. It offers an excellent data source for researches on the spatial scaling effect of LAI retrieved by remote sensing, and is helpful to advance studies in scaling effect. At the same time, it provides a new opportunity for estimating the sowing area and the crops growth.

ACKNOWLEDGMENT

The authors would like to thank the Beijing Landview Mapping Information Technology Company for supplying the DMC+4 multispectral and panchromatic images, and Dr. Liu Q. for providing the TM images used in the study. They would also like to thank Dr. Chen Z. for his help with radiation calibration of the DMC+4 product.

REFERENCES

[1] Verstraete M. M., Pinty B., and Myneni R. B., "Potential and limitations of information extraction on the terrestrial biosphere from satellite remote sensing," Remote Sens. Environ., vol. 58, pp. 201-214, 1996.

[2] Weiss M. and Baret F., "Evaluation of canopy biophysical variable retrieval performances from the accumulation of large swath satellite data," Remote Sens. Environ., vol. 70, pp. 293—306, 1999.

[3] Fang X. and Zhang W., "The application of remotely sensed data to the estimation of the Leaf Area Index," Remote Sensing For Land & Resources, vol. 3, pp. 58-62, 2003.

[4] Tian Q. and Jin Z., "Research on calculation and spatial scaling of forest Leaf Area Index from remote sensing image," Remote Sens. Information, vol. 4, pp. 5–11, 2006.

[5] Yao Y., Yan G. and Wang J., "The approach on Leaf Area Index inversion using multiangular and multispectral data sets," Journal of Remote Sens., vol. 9, pp. 117-122, 2005.

[6] Wang X., Huang J., Li Y. and Wang R., "The study on multi-spectral remote sensing estimation models about LAI of rice," Remote Sens. Technology and Application, vol. 18, pp. 57-65, 2003.

[7] Qu Y., Wang J., Liu S., Wan H., Zhou H. and Lin H., "Study on hybrid inversion scheme under bayesian network," Journal of Remote Sens., vol. 10, pp. 6–14, 2006.

[8] Huo D., Yan M. and Yu B., "Analysis on DMC remotely sensed mini-satellite data pre-processing method," Journal of Remote Sens., vol. 9, pp. 480-485, 2005.

[9] Li B. and Zuo Y., "DMC+4 Micro-satellite application and research in international disaster monitoring," Journal of Remote Sens., vol. 9, pp. 469-471, 2005.

[10] Li X. and Strahler A. H., "Geometric-optical modeling of a conifer forest canopy," IEEE Trans. Geosci. Remote Sens., vol. 23, pp. 705-721, 1985.

[11] Li X. and Strahler A. H., "Geometric-optical bidirectional reflectance modeling of a coniferous forest canopy," IEEE Trans. Geosci. Remote Sens., vol. 24, pp. 906-919, 1986.

[12] Li X. and Strahler A. H., "Geometric-optical bi-directional reflectance modeling of mutual shadowing effects of crowns in a forest canopy," IEEE Trans. Geosci. Remote Sens., vol. 30, pp. 276-292, 1992.

[13] Jupp D. L. B. and Strahler A. H., "A hotspot model for leaf canopies," Remote Sens. Environ., vol. 38, pp. 193-210, 1991.

[14] Strahler A. H. and Jupp D. L. B., "Modeling bi-directional reflectance of forests and woodlands using boolean models and geometric Optics," Remote Sens. Environ., vol. 34, pp. 153-166, 1990.

[15] J. M. Chen, G. Pavlic, L. Brown, J. Cihlar, S. G. Leblanc, H. P. White, et al., "Derivation and validation of Canada-wide coarse-resolution leaf area index maps using high-resolution satellite imagery and ground measurements," Remote Sens. Environ., vol. 80(1), pp. 165-184, 2002.

[16] Nilson T., "A theoretical analysis of the frequency of gaps in plant stands," Agric. Meteorol., vol. 8, pp. 25-38, 1971.

[17] Nilson T. and Kuusk A., "A reflectance model for the homogeneous plant canopy and its inversion," Remote Sens. Environ., vol. 27, pp. 157-167, 1989.

[18] Hapke B. W., "Bi-directional reflectance spectroscopy, 1, theory," J. Geophys. Res., vol. 86, pp. 3039-3054, 1981.

[19] Liu Q. and Xu X., "Matching of airphotos with TM images and precision testing of crop area estimation by means of TM using airphotos," Journal of Remote Sens., vol. 9, pp. 275-277, 1994.